Supplementary Information

Trade-off between H$_2$O-rich and H$_2$O-poor electric double layers enables highly reversible Zn anodes in aqueous Zn-ion batteries

Kaiwen Qi,[a] Pengrui Liang,[a] Shiqiang Wei,[b] Huaisheng Ao,[c] Xuan Ding,[a] Shiyuan Chen,[a] Zhechen Fan,[a] Chengming Wang,[a] Li Song,[b] Xiaojun Wu,[a] Changzheng Wu*[a] and Yongchun Zhu*[a]*

[a] School of Chemistry and Materials Science, University of Science and Technology of China, Hefei 230026, P.R. China

[b] National Synchrotron Radiation Laboratory, CAS Center for Excellence in Nanoscience, University of Science and Technology of China, Hefei 230029, P. R. China

[c] School of Petrochemical Engineering, Changzhou University, Changzhou, 213164, P.R. China

*Corresponding Author: xjwu@ustc.edu.cn, czwu@ustc.edu.cn, ychzhu@ustc.edu.cn

Experimental Methods

Preparation of Electrolytes. Different concentrations of aspartame (APM) (0, 0.1, 1, and 10 mM) were respectively added in the 2 M $ZnSO_4$ and ultrasonicated until completely dissolved to obtain a series of electrolytes.

Preparation of CNT/MnO$_2$ Composites. 0.25 g of carboxylated multi-walled CNTs were dispersed in aqueous solution of $Mn(CH_3COO)_2 \cdot 4H_2O$ (1.69 g/20 mL) and ultrasonicated for 30 min. Then, the prepared $KMnO_4$ (0.727 g/60 mL) solution was added into the above mixed solution and stirring for 30 min. The resulting solution was then heated to 80°C under continuous magnetic stirring for 6 h and naturally cooled to room temperature. Finally, the resulting solid product (CNT/MnO_2) was filtered and washed 3 times with deionized water and dried at 80°C for 12 hours.

Preparation of NH$_4$V$_4$O$_{10}$. 18 mM NH_4VO_3 and 27 mM $H_2C_2O_4 \cdot 2H_2O$ were dispersed in 90 mL deionized water at 80 °C. The mixture was then transferred to a Teflon-lined autoclave and heated at 140 °C for 48 h. The obtained product was collected by filtration, washed with deionized water and ethanol, and ultimately dried at 70 °C.

Characterization. The structures of the samples were measured by X-ray diffraction (XRD) on a Philips X' Pert Super diffractometer with Cu K_α (λ=1.54182 Å). FT-IR tests were performed on a Hyperion 3000 system. Raman spectra were characterized using a JYLABRAM-HR confocal laser micro-Raman spectrometer at a wavelength of 532 nm. The morphologies and elemental mapping for the samples were characterized by scanning electron microscopy (SEM, Gemini 450). Operando visualization of Zn deposition behavior was carried out by optical microscope (YUESCOPE YM-520TR). The contact angle between zinc foil and electrolyte was measured using a contact angle measuring instrument (SL200HP). The ionic conductivity of different electrolytes was collected through a conductivity meter (DDS-11A). The pH value of different electrolytes was measured by pH meter (PHS-3C).

Electrochemical Measurements. The electrochemical performance of symmetric cells and half-cells was measured using CR2016 coin cells containing glass fiber separator (Whatman, GF/C) and 2 M $ZnSO_4$ electrolyte. The galvanostatic charge/discharge performance was tested using LAND CT2001A and NEWARE CT4008T battery testers. The electrochemical impedance spectroscopy (EIS) was recorded on a CHI 660E electrochemical workstation with a frequency ranging from 100 kHz to 0.01 Hz with an amplitude of 5 mV. In the alternating current voltammetry tests, the frequency is 6 Hz and the amplitude is 5 mV, with a potential range extended from 0.7 to 0.1 V versus Zn/Zn^{2+} and the selective region of phase angles was 0 and 90°. The Electric double-layer capacitance (EDLC) measurements were obtained by measuring CV of Zn||Zn symmetric cells in different electrolytes at different sweep rates (2-10 mV s$^-$^{1}) in the non-Faraday interval (±15 mV). EDLC was calculated by the equation of $C=i_c/v$, where C is the capacitance, i_c is the double layer current, v is the scan rate. The capacitance (C) can be obtained from the slope of the i_c versus v. Here, we define i_c as the half value of the current difference during the forward

scan and negative scan at 0 V, that is (i_{0V}+ - i_{0V}-)/2. The cyclic voltammetry (CV) was performed with a scan rate of 1 mV s^{-1} and 0.1 mV s^{-1} for half-cells and full cells, respectively. Linear sweep voltammetry (LSV) was performed with three-electrode system using Zn anode as working electrode, platinum as counter electrode and Ag/AgCl as reference electrode in 1 M $NaSO_4$ aqueous solution with/without APM additive. The average CE was measured using the modified Aurbach method while the current density was fixed at 0.5 mA cm^{-2}. The initial pre-cycle was performed to 5 mA h cm^{-2}, followed by the deposition of 5 mA h cm^{-2} Zn (Q_R, amount of charge). The final stripping (cut-off voltage: 0.7 V) was performed (Q_S, amount of charge) after 10 plating/stripping cycles to 1 mA h cm^{-2}. Therefore, the average CE is calculated as follows:

$$Average\ CE(\%) = \frac{(Q_S + 1 \times 10)mA\ h\ cm^{-2}}{(Q_R + 1 \times 10)mA\ h\ cm^{-2}} \times 100\%$$

Linear polarization measurements and chronoamperometry (CA) were conducted in symmetrical cells. The CNT/MnO_2 and $NH_4V_4O_{10}$ cathodes were fabricated with active materials, Ketjen Black, polyvinylidene fluoride in a weight ratio of 7:2:1. The assembled full cells were initially activated with one-tenth of the applied current prior to formal test, and then were subjected to long-term cyclic stability testing within the voltage range of 0.85-1.85 V and 0.4-1.4 V (vs. Zn^{2+}/Zn) for $Zn\|CNT/MnO_2$ and $Zn\|NH_4V_4O_{10}$ full cells, respectively.

Computational Details

The geometry optimizations, energy calculations and electrostatic potential (ESP) for APM and H_2O were performed by implementing the Gaussian 16 (C. 01) program package, using B3LYP exchange-correlation functional in conjunction with the 6-31g(d) basis set. The Integral Equation Formalism Polarizable Continuum Model (IEFPCM) implicit solvation model was used to describe the solvation effect.

The adsorption energy were determined using density functional theory (DFT) calculations with the Vienna Ab Initio Package (VASP).[1] The Perdew-Burke-Enzerhof (PBE) exchange correlation function of the generalized gradient approximation (GGA) and projected augmented wave (PAW) pseudopotentials were applied, according to previous research.[2] The energy cutoff of 400 eV was used for the plane wave expansion of valence electron wave function. Brillouin zone sampling were performed using the 2×2×1 gamma k-mesh scheme with a reciprocal space discretization of 0.04 $Å^{-1}$. The Grimme's method (DFT-D3) was employed to incorporate the effects of van der Waals interactions. To minimize the interactions between the molecules. The supercells (23.329 Å×15.760 Å) of Zn (101) surface and (15.760 Å×15.760 Å) of Zn (001) surface with four Zn layers and 20 Å vacuum were selected to simulate the adsorption systems. The energy convergence condition was 10^{-6} eV, and the force convergence was set to 0.05 eV $Å^{-1}$. The adsorption energy (E_{ads}) of molecule on the Zn layer was calculated as follows: $E_{ads} = E_{total} - (E_{slab} + E_{molecule})$ where E_{total} and E_{slab} stand for the total energy of slabs with and without adsorbed molecule while the $E_{molecule}$ refers to the energy of the molecule (APM or H_2O).

Supplementary Figures
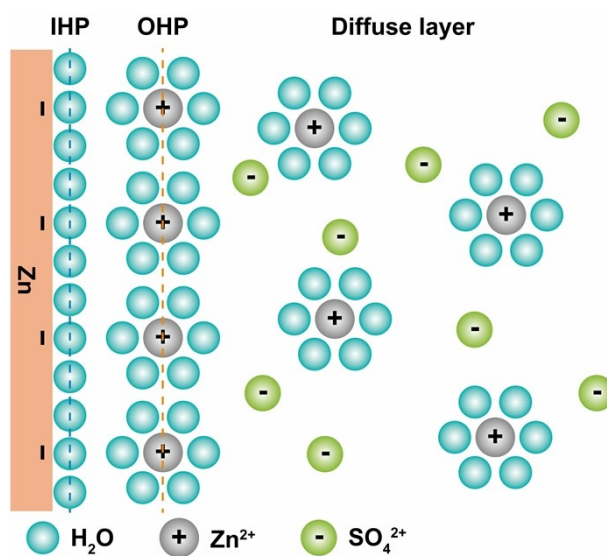
Fig. S1 Schematic illustrations of the EDL structure at Zn anode/electrolyte interface in 2 M $ZnSO_4$ electrolyte.
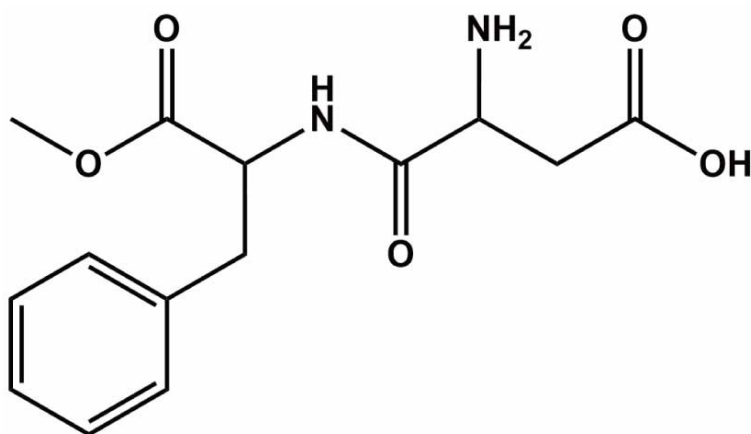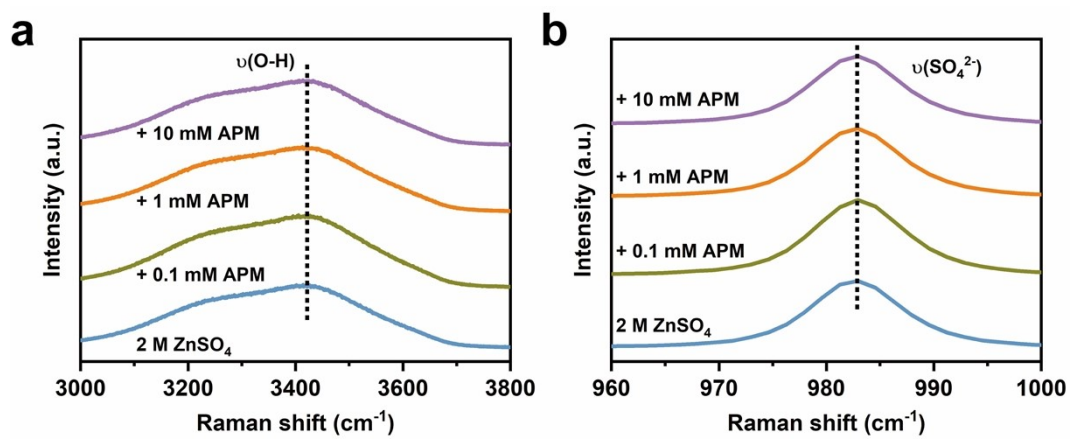

Fig. S2 Molecular structure of aspartame.

Fig. S3 Raman spectra of different electrolytes.
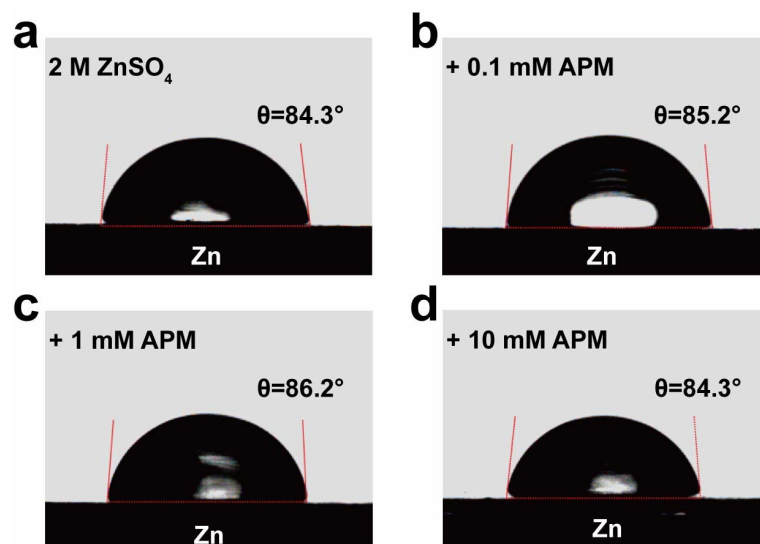

Fig. S4 The contact angles of (a) 2 M $ZnSO_4$ and 2 M $ZnSO_4$ + (b) 0.1, (c) 1 and (d) 10 mM APM electrolytes.
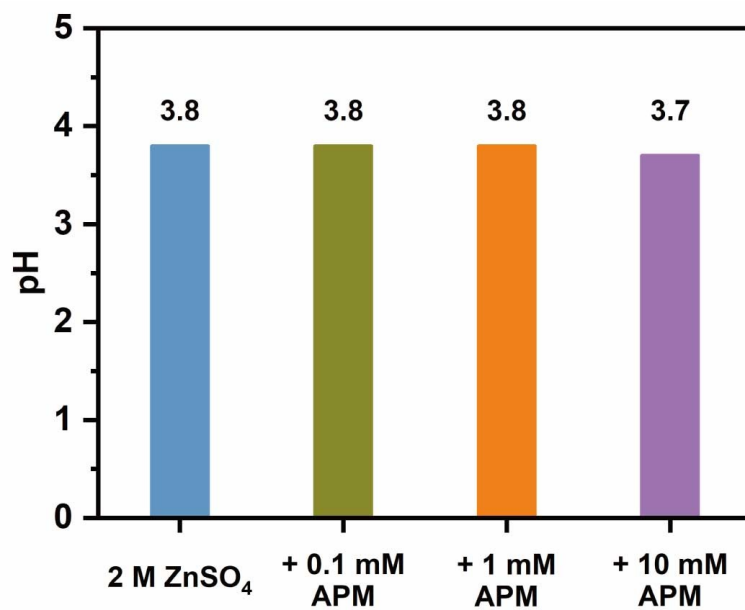
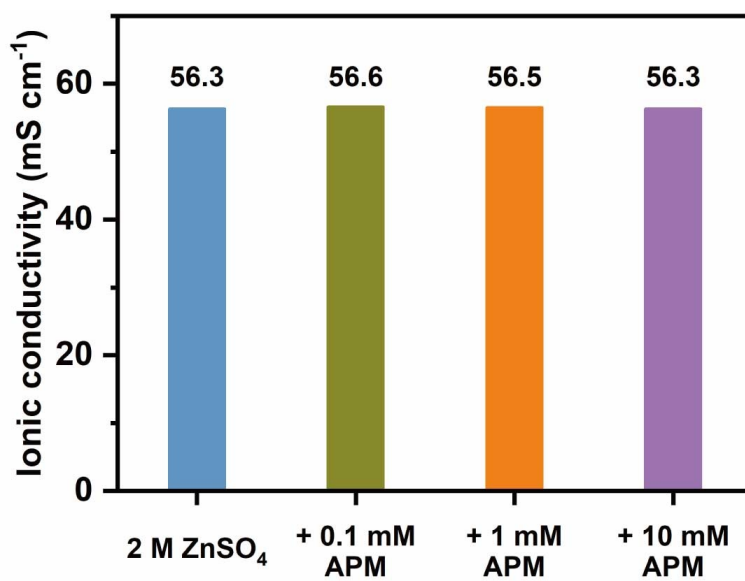**Fig. S5** pH value of different electrolytes.
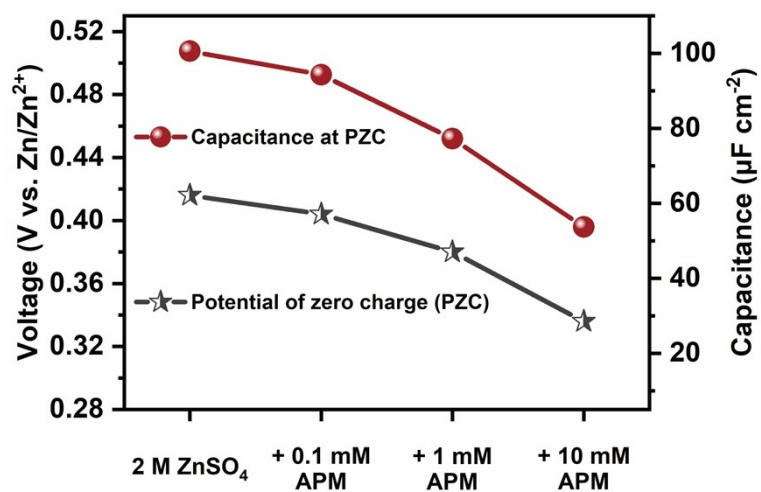

Fig. S6 Ionic conductivity of different electrolytes.

Fig. S7 The PZC and the capacitance at PZC of Zn||Cu half-cells using different electrolytes.
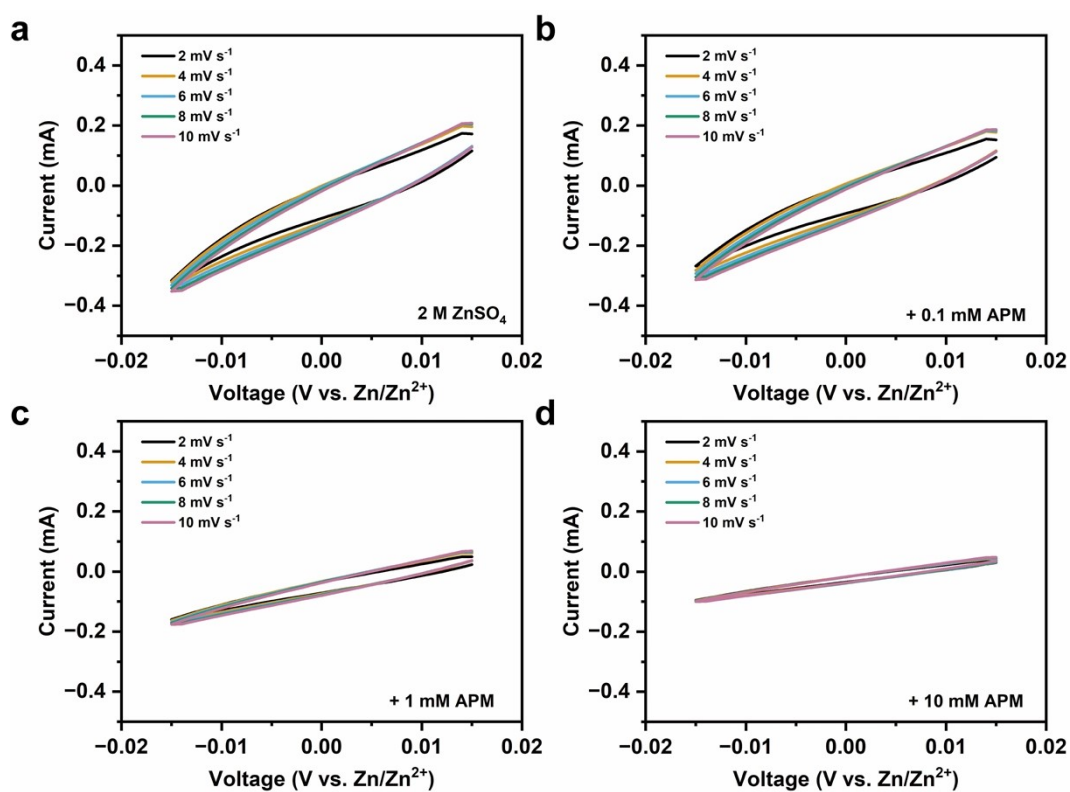
Fig. S8 CV curves of Zn||Zn symmetric cells using different electrolytes under various scanning rates.
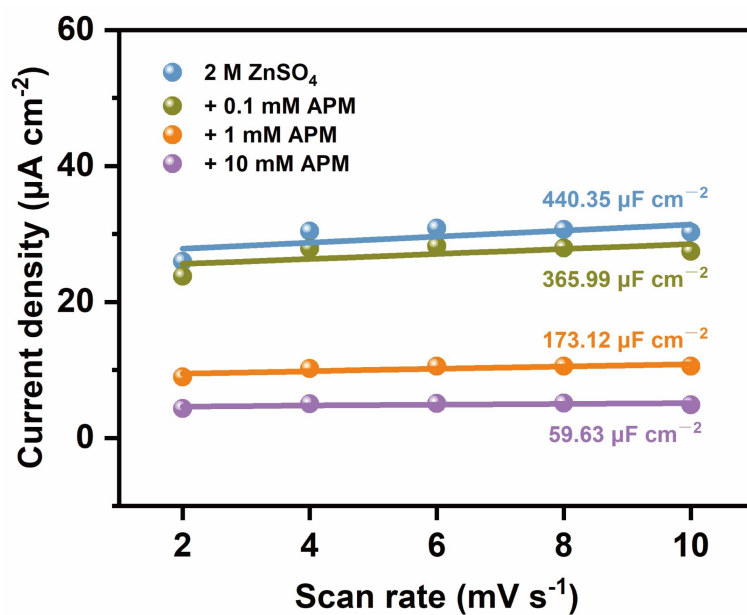
Fig. S9 Plots of capacitive currents versus scan rate.

a -1030.008358	**b** -1030.008711	**c** -1030.008358	**d** -1030.00863	**e** -1030.008711
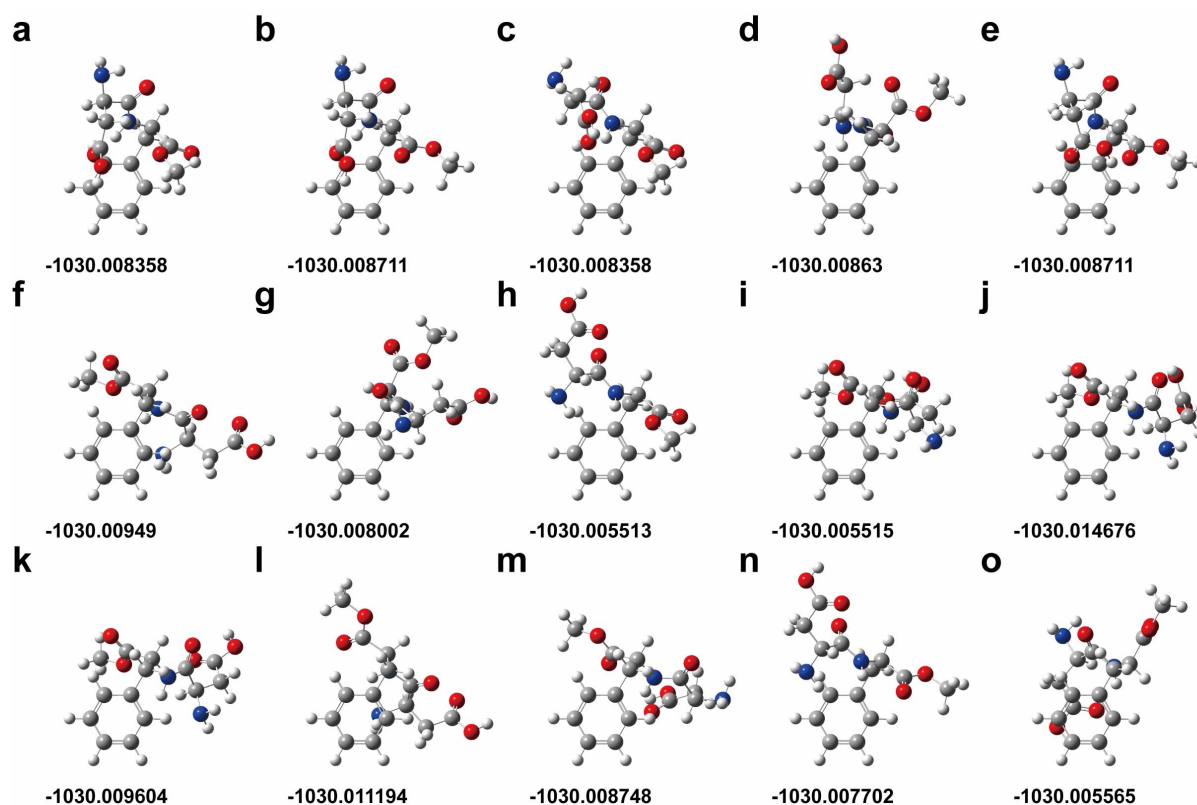
Fig. S10 The geometries for various conformers of APM considered in this work and their total energies (Unit: Hartree) in water solvent.

a   -1030.008358
b   -1030.008711
c   -1030.008358
d   -1030.00863
e   -1030.008711

f   -1030.00949
g   -1030.008002
h   -1030.005513
i   -1030.005515
j   -1030.014676

k   -1030.009604
l   -1030.011194
m   -1030.008748
n   -1030.007702
o   -1030.005565
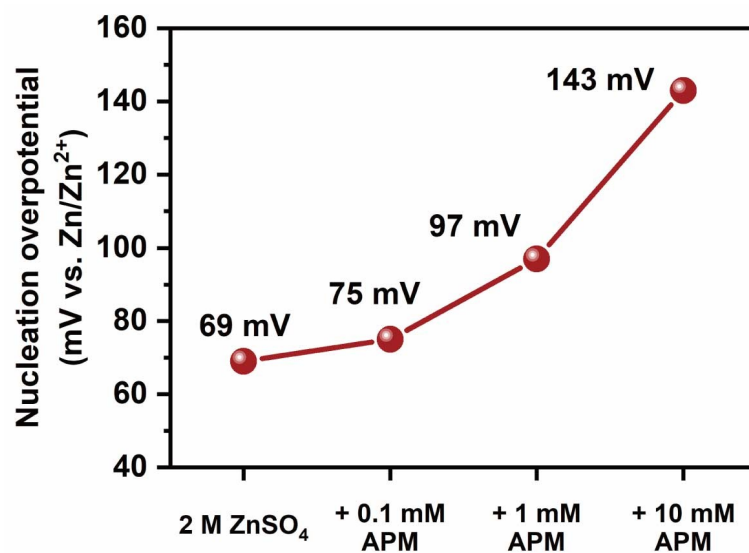
Fig. S11 The nucleation overpotential of Zn‖Cu half-cells using different electrolytes.
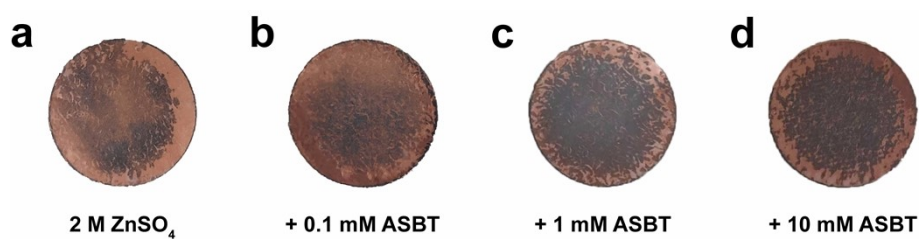
Fig. S12 Digital photographs for Cu metal surface of Zn‖Cu half-cells using different electrolytes after plating at 0.5 mA cm^{-2} for 2 mA h.
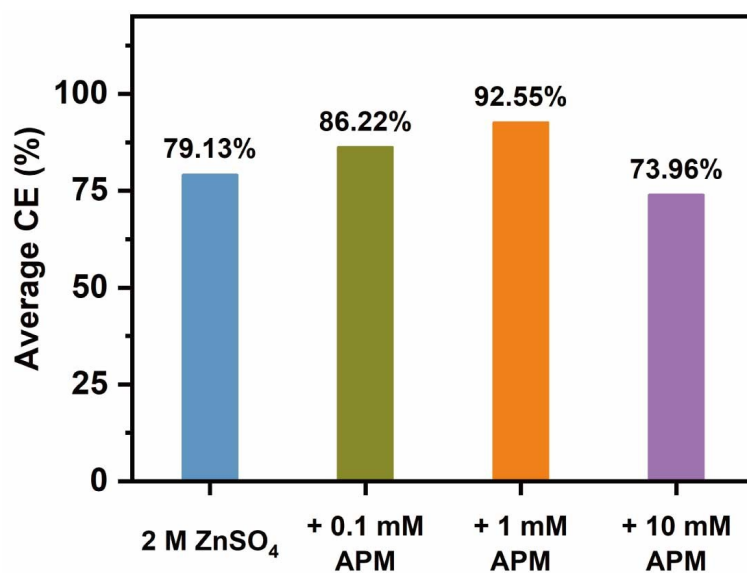
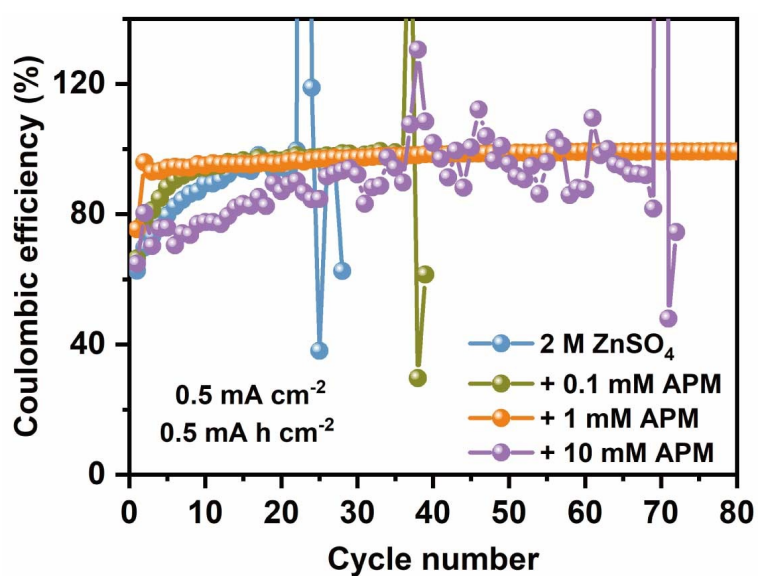**Fig. S13** Average CE of initial 10 cycles in half-cells using different electrolytes.

Fig. S14 The enlarged details of Zn‖Cu half-cells performance in different electrolyte at initial several cycles.
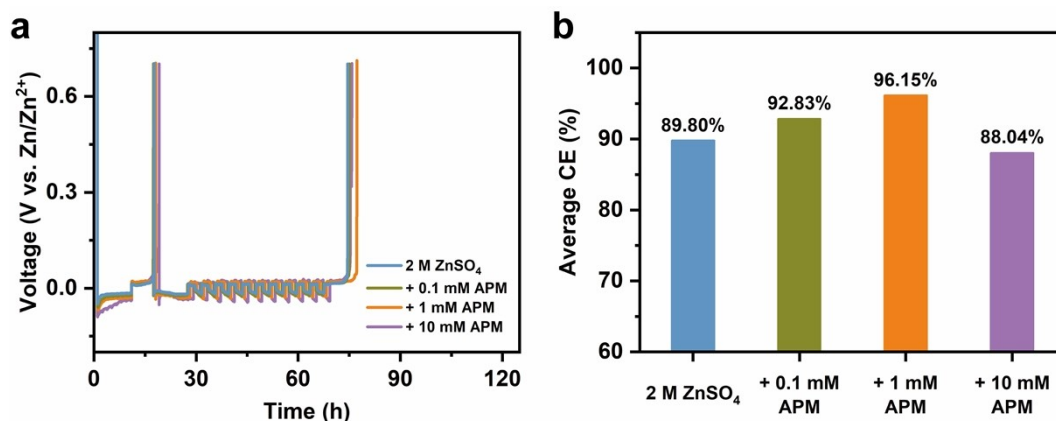
Fig. S15 (a) Time versus voltage curves and (b) average CE of Zn‖Cu half-cells using different electrolytes under the modified Aurbach method.
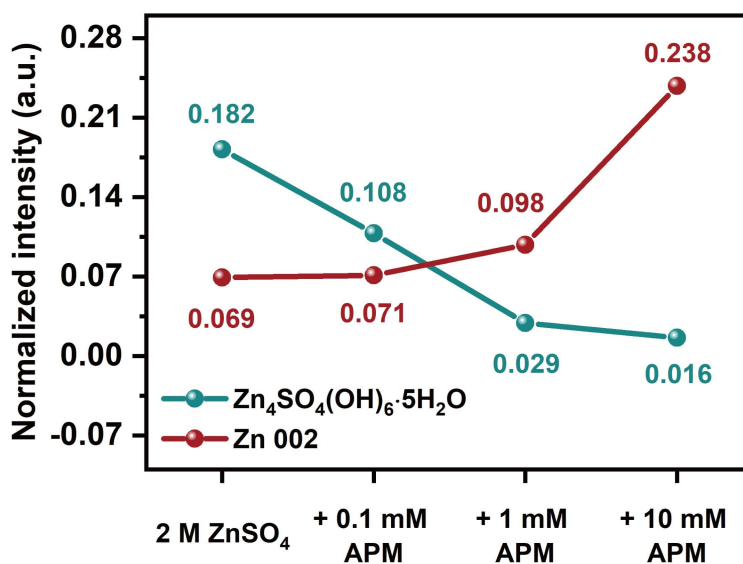
Fig. S16 Normalized intensity of the characteristic peaks of $Zn_4SO_4(OH)_6 \cdot 5H_2O$ and Zn 002 on Cu metal surfaces in Zn‖Cu half-cells using different electrolytes after 10 cycles at 0.5 mA cm^{-2} and 0.5 mA h cm^{-2}.
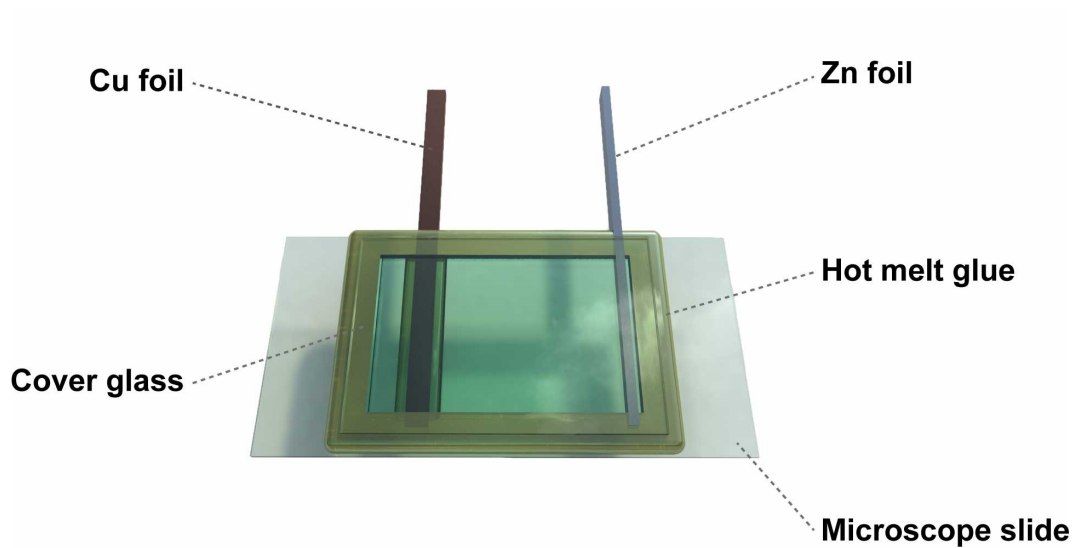
Fig. S17 Schematic diagram of self-designed transparent Zn∥Cu cell for *in situ* optical microscopy monitoring.
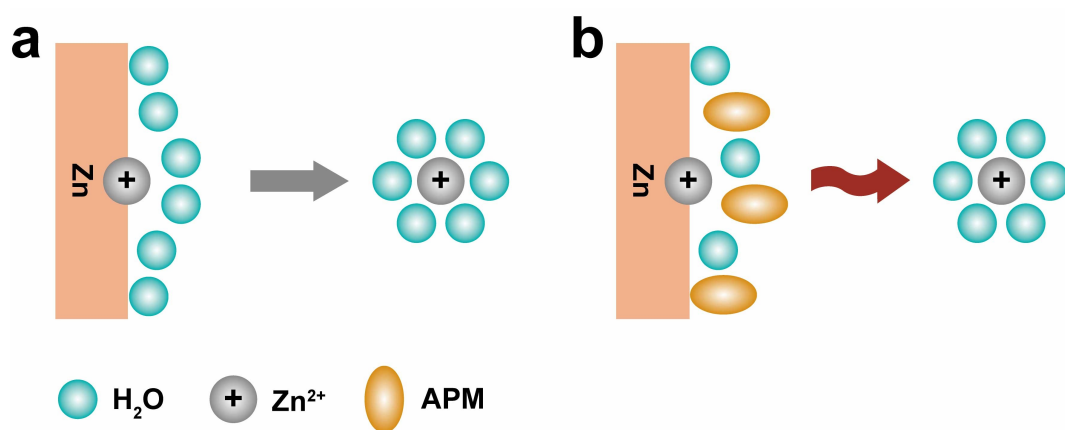

H_2O Zn^{2+} APM

Fig. S18 Schematic diagram for the solvation of Zn^{2+} ions during Zn stripping in (a) H_2O-rich EDL and (b) H_2O-poor EDL.
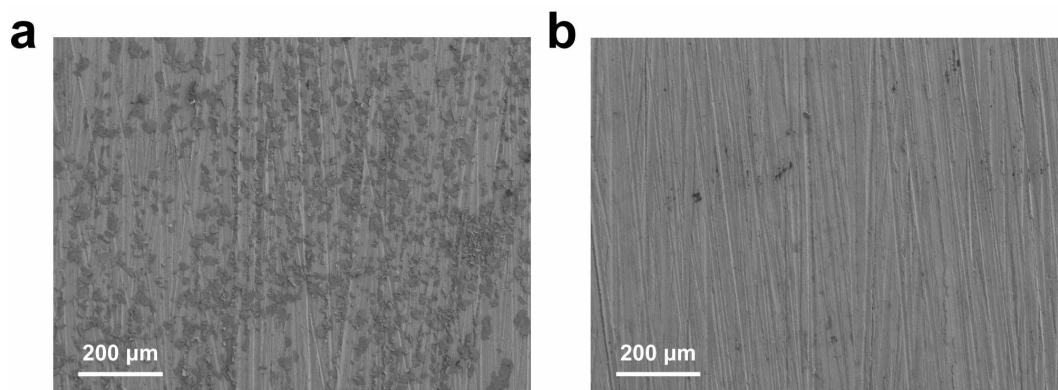
Fig. S19 SEM images of Zn metal surfaces after soaking in (a) 2 M $ZnSO_4$ and (b) 2 M $ZnSO_4$ + 1mM APM electrolytes for 3 days.
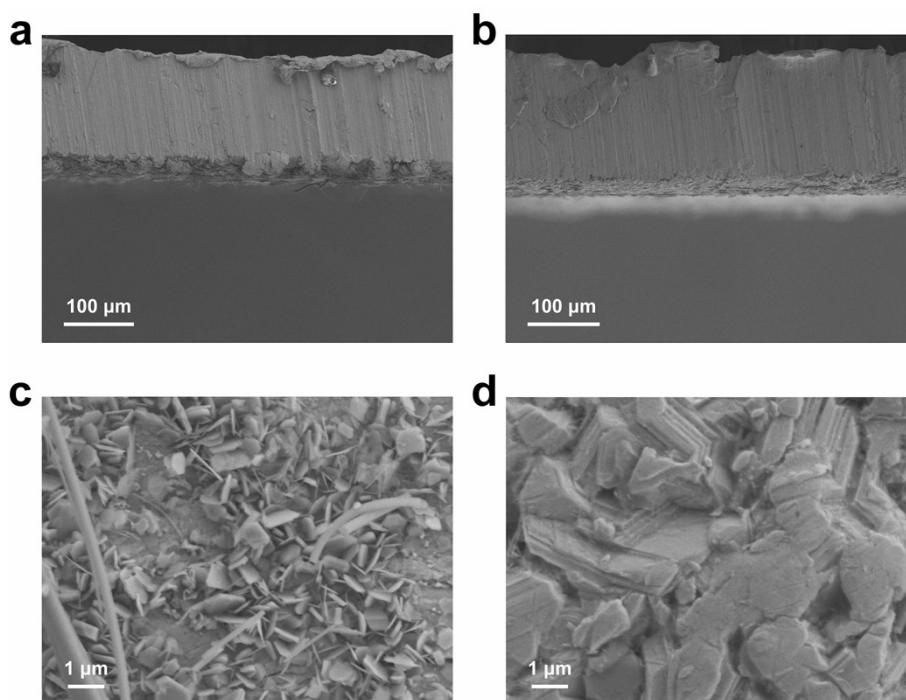

Fig. S20 SEM images of Zn metal surfaces after plating in Zn symmetric cells using (a, c) 2 M $ZnSO_4$ and (b, d) 2 M $ZnSO_4$ + 1mM APM electrolytes.
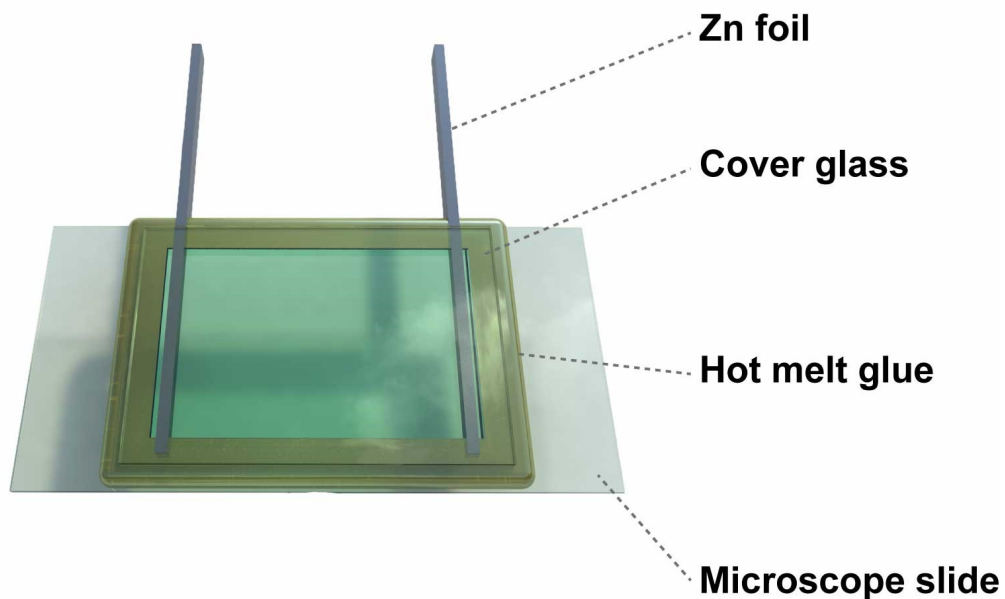
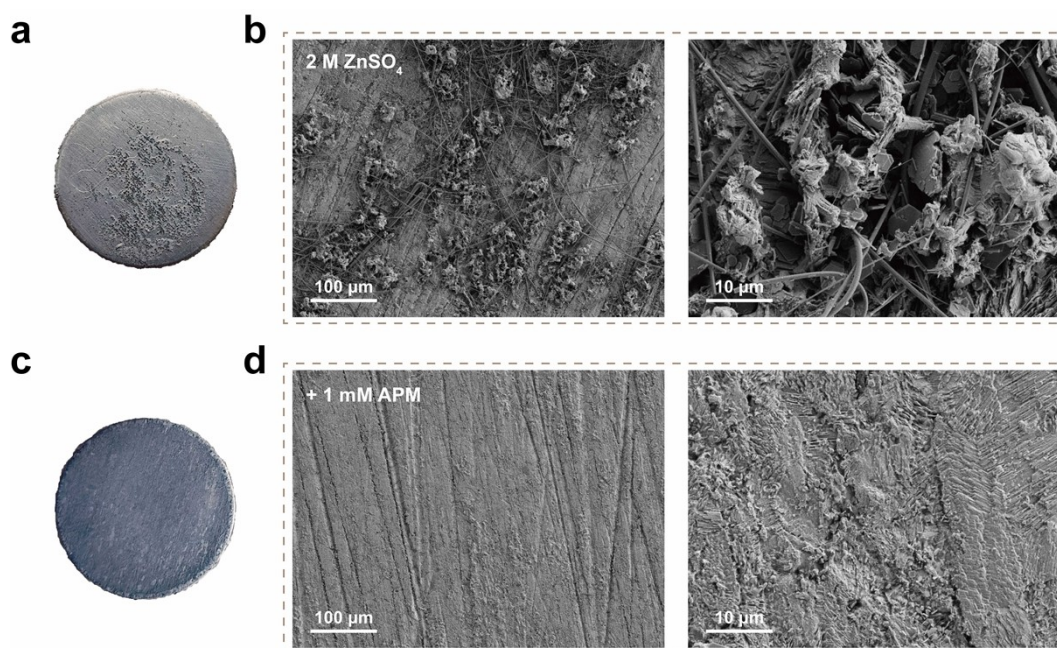**Fig. S21** Schematic diagram of self-designed transparent Zn||Zn cell for *in situ* optical microscopy monitoring.

Fig. S22 Digital photographs and SEM images of Zn metal surface in Zn symmetric cells using (a, b) 2 M ZnSO$_4$ and (c, d) 2 M ZnSO$_4$ + 1mM APM electrolytes after 20 cycles at 0.5 mA cm^{-2} and 0.5 mA h cm^{-2}.
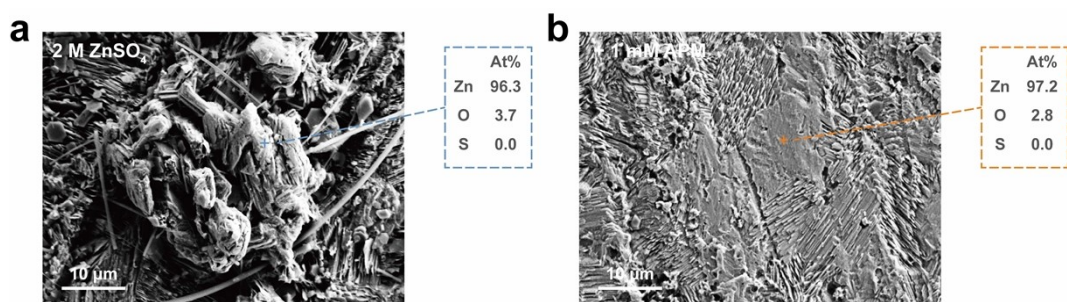
Fig. S23 SEM images and EDS elemental quantification results of the area on Zn surface not covered by ZHS in Zn symmetric cells using (a) 2 M ZnSO$_4$ and (b) 2 M ZnSO$_4$ + 1mM APM electrolytes after 20 cycles at 0.5 mA cm^{-2} and 0.5 mA h cm^{-2}.
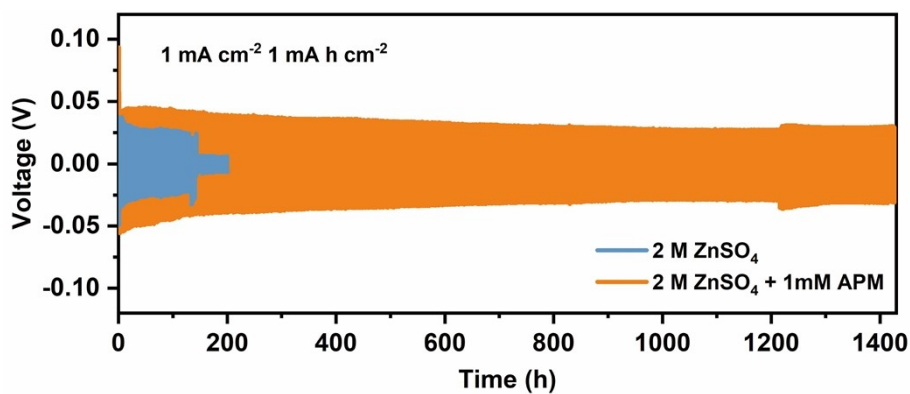

Fig. S24 Long-term galvanostatic cycling of Zn||Zn symmetric cells at a current density of 1 mA cm^{-2} with a capacity of 1 mA h cm^{-2}.
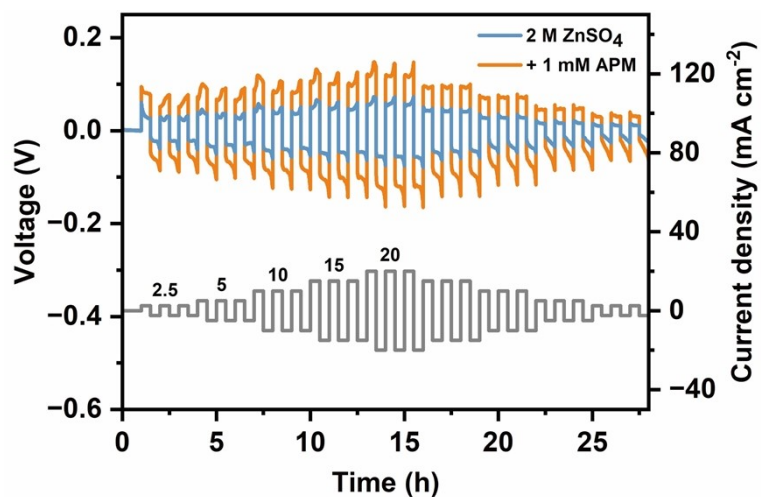
Fig. S25 Rate performance of symmetric cells using different electrolytes charging/discharging at various current densities.
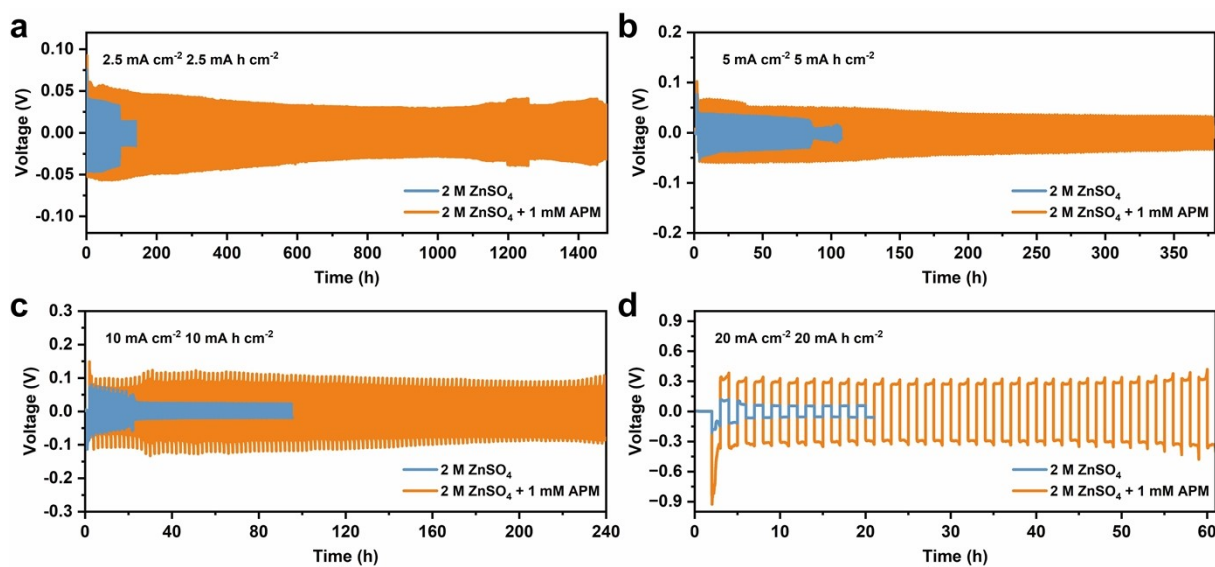

Fig. S26 Long-term galvanostatic cycling of Zn||Zn symmetric cells at a current density of (a) 2.5, (b) 5, (c) 10 and (d) 20 mA cm^{-2} with a capacity of 2.5, 5, 10 and 20 mA h cm^{-2}, respectively.
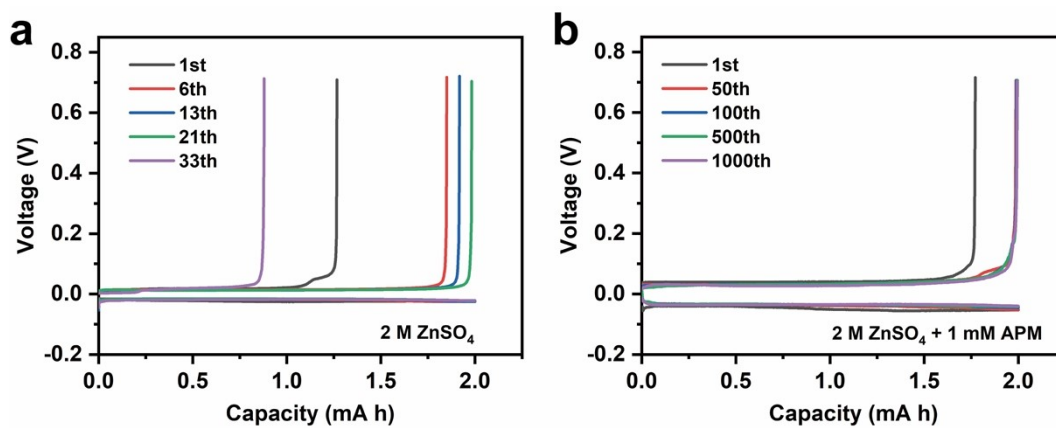
Fig. S27 The charge−discharge voltage profiles of Zn‖Cu half-cells using (a) 2 M ZnSO$_4$ and (b) 2 M ZnSO$_4$ + 1mM APM electrolytes at 1 mA cm^{-2} and 1 mA h cm^{-2}.
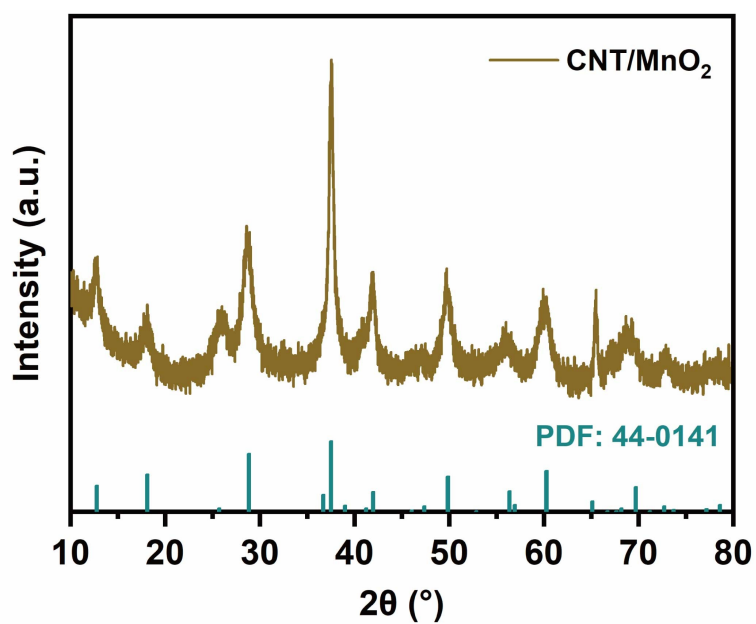

Fig. S28 XRD patterns of CNT/MnO$_2$.

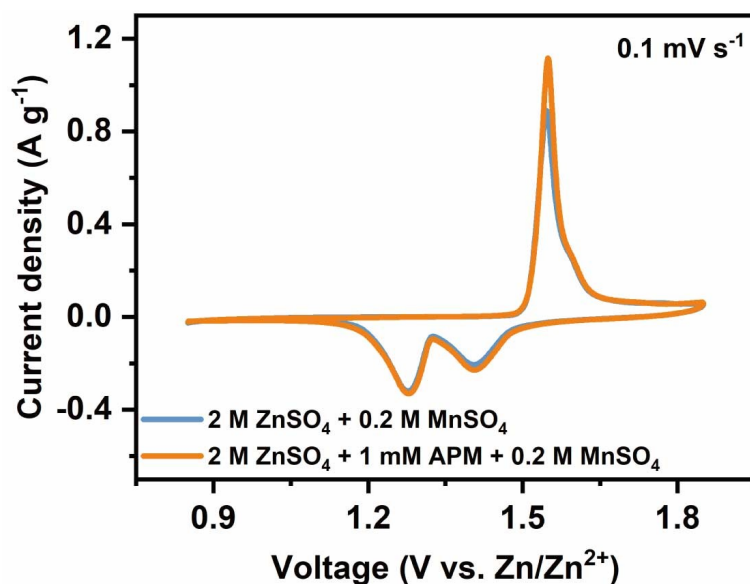**Fig. S29** CV curves of Zn‖CNT/MnO$_2$ cells using different electrolytes.
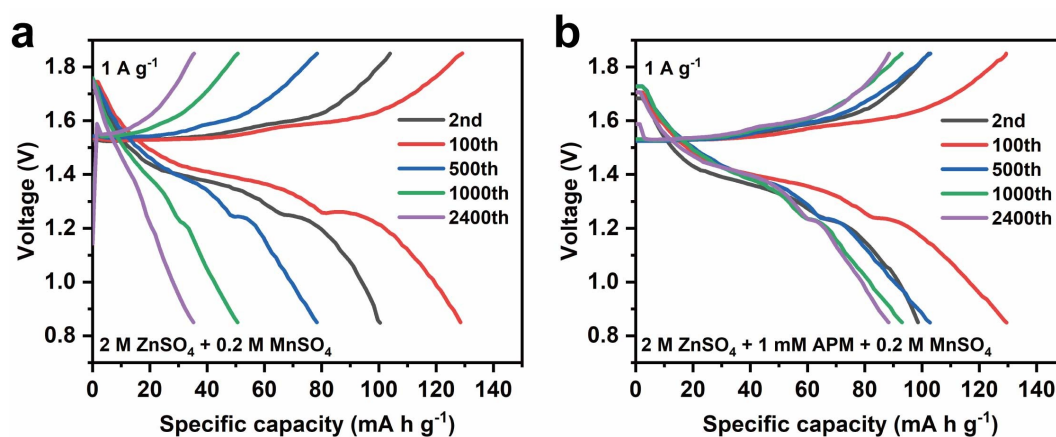
Fig. S30 GCD curves of Zn‖CNT/MnO$_2$ cells using (a) 2 M ZnSO$_4$ + 0.2 M MnSO$_4$ and (b) 2 M ZnSO$_4$ + 1mM APM + 0.2 M MnSO$_4$ electrolytes at different cycles.
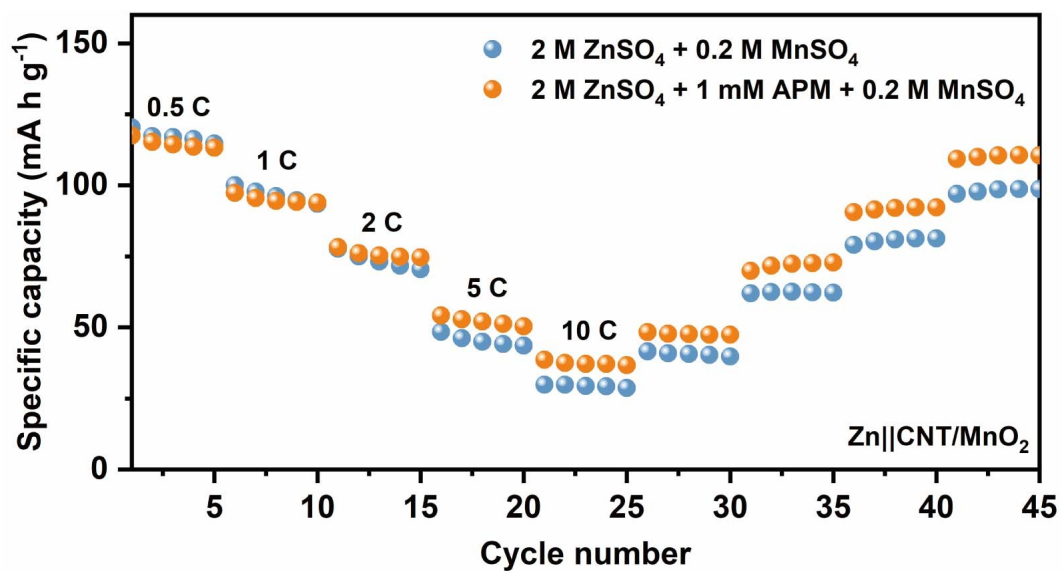
Fig. S31 Rate performance of Zn‖CNT/MnO$_2$ cells using different electrolytes.

Fig. S32 XRD patterns of NH$_4$V$_4$O$_{10}$.

Fig. S33 CV curves of Zn‖NH₄V₄O₁₀ cells using different electrolytes.

Fig. S34 GCD curves of Zn‖NH₄V₄O₁₀ cells using (a) 2 M ZnSO₄ and (b) 2 M ZnSO₄ + 1mM APM electrolytes at different cycles.
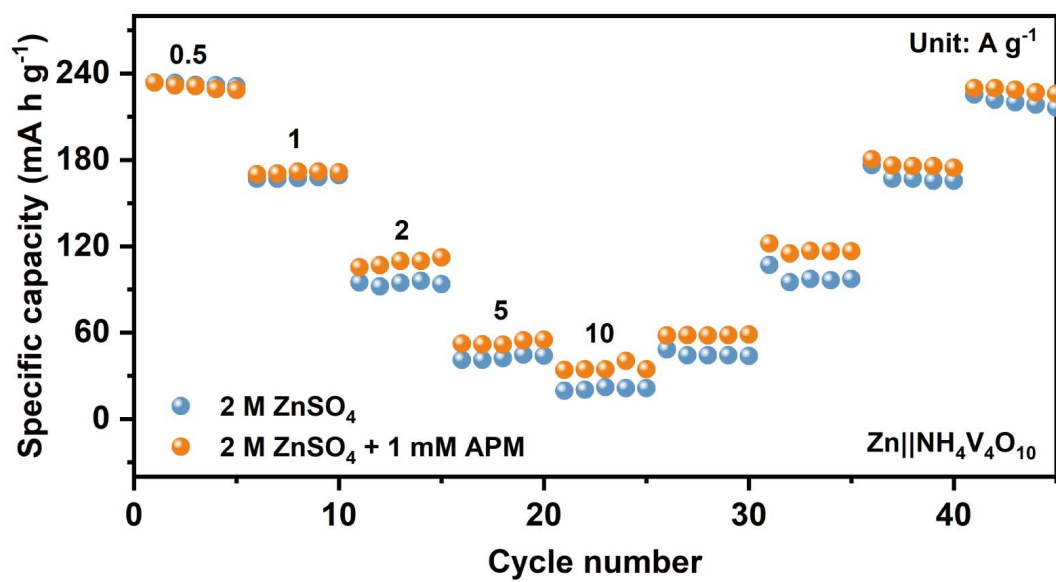
Fig. S35 Rate performance of Zn||NH$_4$V$_4$O$_{10}$ cells using different electrolytes.
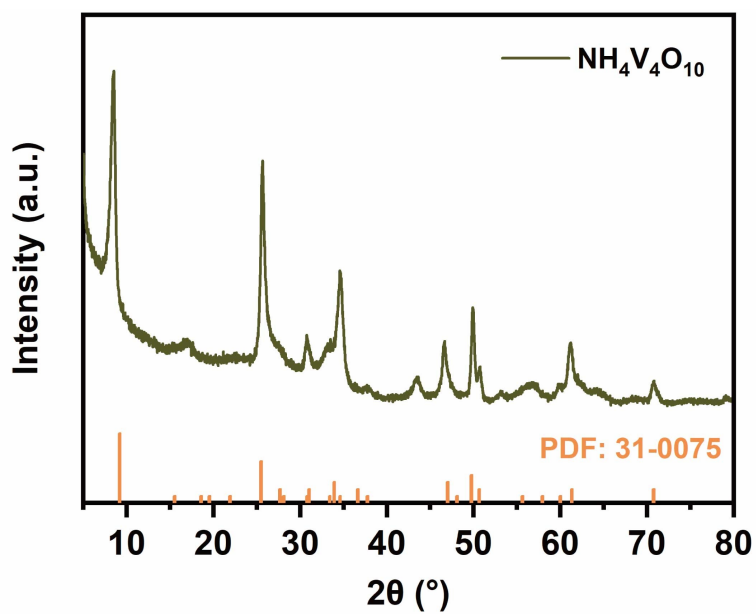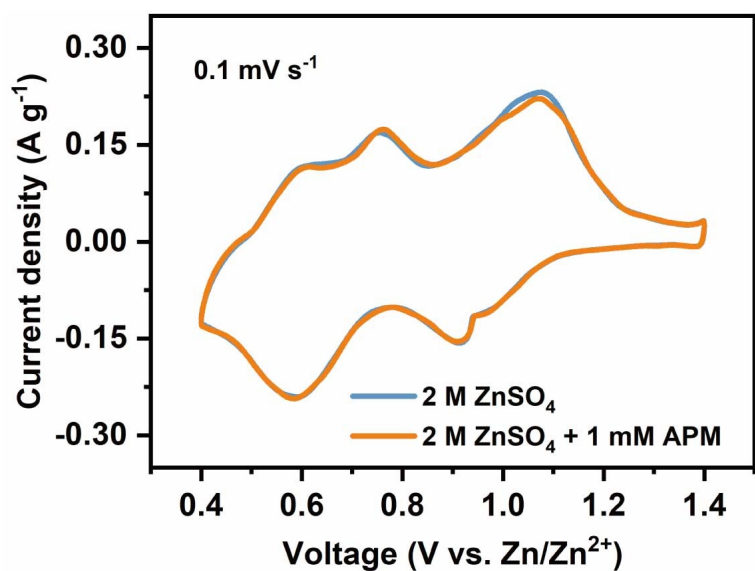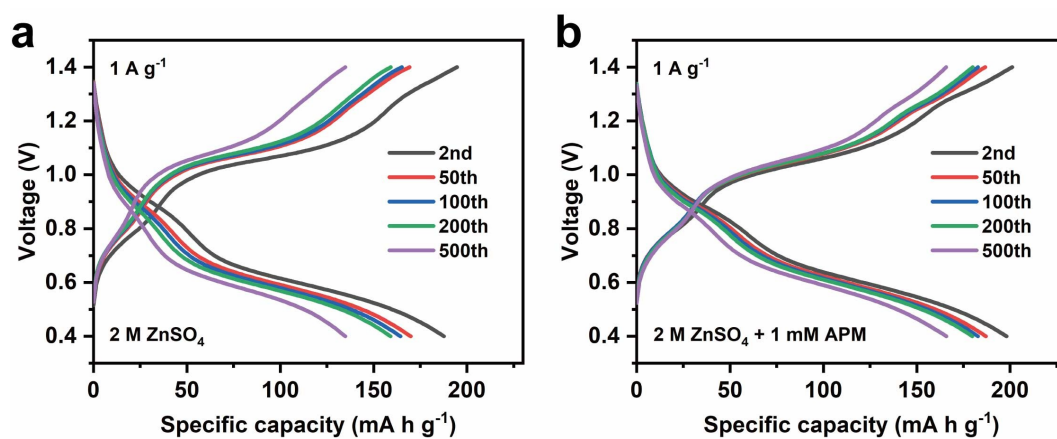
Supplementary Tables

Table S1. Comparison of accumulated capacity for Zn‖Zn symmetric cell in this work with other reported works.

Reference	Current density (mA cm^{-2})	Capacity (mA h cm^{-2})	Accumulated capacity (mA h cm^{-2})
This work	5	1	5950
Ref. a[3]	5	1	3950
Ref. b[4]	5	1	2750
Ref. c[5]	5	1	2500
Ref. d[6]	5	1	1750
Ref. e[7]	5	1	1250
Ref. f[8]	6	1.5	2400
Ref. g[9]	5	5	1375
Ref. h[10]	5	2.5	2500
Ref. i[11]	5	2.5	1500
Ref. j[12]	4	4	700
Ref. k[13]	2	2	2000
Ref. l[14]	2	1	2600
Ref. m[15]	2	1	1500
Ref. n[16]	1	1	1000
Ref. o[17]	1	1	1150
Ref. p[18]	1	1	600
Ref. q[19]	1	0.5	1250
Ref. r[20]	0.5	0.5	875
Ref. s[21]	0.5	0.5	825
Ref. t[22]	0.5	0.25	375

References

1   G. Kresse and J. Furthmuller, *Phys. Rev. B*, 1996, **54**, 11169-11186.

2   Y. Y. Lai, H. X. Xie, P. Li, B. Li, A. Zhao, L. B. Luo, Z. W. Jiang, Y. J. Fang, S. L. Chen, X. P. Ai, D. G. Xia and Y. L. Cao, *Adv. Mater.*, 2022, **34**, 202206039.

3   H. Zheng, Y. Huang, J. Xiao, W. P. Zeng, X. P. Li, X. Li, M. S. Wang and Y. H. Lin, *Chem. Eng. J.*, 2023, **468**, 143834.

4   R. Sun, D. L. Han, C. J. Cui, Z. S. Han, X. X. Guo, B. Zhang, Y. Guo, Y. X. Liu, Z. Weng and Q. H. Yang, *Angew. Chem. Int. Ed.*, 2023, **62**, e202303557.

5   X. J. Lu, Z. H. Liu, A. Amardeep, Z. R. Wu, L. Tao, K. Q. Qu, H. Sun, Y. L. Liu and J. Liu, *Angew. Chem. Int. Ed.*, 2023, **62**, e202307475.

6   F. H. Yang, J. A. Yuwono, J. N. Hao, J. Long, L. B. Yuan, Y. Y. Wang, S. L. Liu, Y. M. Fan, S. Y. Zhao, K. Davey and Z. P. Guo, *Adv. Mater.*, 2022, **34**, 2206754.

7   H. Y. Wu, W. Yan, Y. M. Xing, L. Li, J. Y. Liu, L. Li, P. Huang, C. Lai, C. Wang, W. H. Chen and S. L. Chou, *Adv. Funct. Mater.*, 2023, **34**, 2206754.

8   M. Q. Liu, L. Yao, Y. C. Ji, M. Z. Zhang, Y. L. Cai, H. Y. Li, W. G. Zhao, Y. Zhao, Z. X. Zou, R. Z. Qin, Y. T. Wang, L. L. Liu, H. Liu, T. S. Miller, F. Pan, J. L. Yang, Y. H. Gan and K. Yang, *Nano Lett.*, 2023, **23**, 541-549.

9   H. Cao, X. Q. Zhang, B. Xie, X. M. Huang, F. Y. Xie, Y. Huo, Q. J. Zheng, R. Y. Zhao, Q. Hu, L. Kang, S. D. Liu and D. M. Lin, *Adv. Funct. Mater.*, 2023, **33**, 2305683.

10   S. Q. Jiao, J. M. Fu, Q. F. Yin, H. M. Yao and H. B. Hu, *Energy Storage Mater.*, 2023, **59**, 102774.

11   H. Yang, D. Chen, R. Z. Zhao, G. Y. Li, H. Xu, L. Li, X. Liu, G. S. Li, D. L. Chao and W. Han, *Energy Environ. Sci.*, 2023, **16**, 2910-2923.

12   C. Li, A. Shyamsunder, A. G. Hoane, D. M. Long, C. Y. Kwok, P. G. Kotula, K. R. Zavadil, A. A. Gewirth and L. F. Nazar, *Joule*, 2022, **6**, 1103-1120.

13   X. Yang, Z. Zhang, M. Wu, Z. P. Guo and Z. J. Zheng, *Adv. Mater.*, 2023, **35**, 2303550.

14   Z. Q. Hu, F. L. Zhang, Y. Zhao, H. R. Wang, Y. X. Huang, F. Wu, R. J. Chen and L. Li, *Adv. Mater.*, 2022, **34**, 2203104.

15   Z. Q. Hu, F. L. Zhang, A. B. Zhou, X. Hu, Q. Y. Yan, Y. H. Liu, F. Arshad, Z. J. Li, R. J. Chen, F. Wu and L. Li, *Nano-Micro Letters*, 2023, **15**, 171.

16   S. Chen, D. L. Ji, Q. W. Chen, J. Z. Ma, S. Q. Hou and J. T. Zhang, *Nat. Commun.*, 2023, **14**, 3526.

17   X. Zhao, Y. Wang, C. Huang, Y. Gao, M. Huang, Y. Ding, X. Wang, Z. Si, D. Zhou and F. Kang, *Angew. Chem. Int. Ed.*, 2023, **62**, e202312193.

18   R. R. Zhao, H. F. Wang, H. R. Du, Y. Yang, Z. H. Gao, L. Qie and Y. H. Huang, *Nat. Commun.*, 2022, **13**, 3252.

19   D. M. Li, Y. Tang, S. Q. Liang, B. A. Lu, G. Chen and J. Zhou, *Energy Environ. Sci.*, 2023, **16**, 3381-3390.

20   J. W. Li, S. Zhou, Y. N. Chen, X. Y. Meng, A. Azizi, Q. He, H. Li, L. Chen, C. Han and A. Q. Pan, *Adv. Funct. Mater.*, 2023, **33**, 2307201.

21   L. Zhou, R. Yang, S. Xu, X. Lei, Y. Zheng, J. Wen, F. Zhang and Y. Tang, *Angew. Chem. Int. Ed.*, 2023, **62**, e202307880

22   J. D. Wan, R. Wang, Z. X. Liu, L. H. Zhang, F. Liang, T. F. Zhou, S. L. Zhang, L. Zhang, Q. Q. Lu, C. F. Zhang and Z. P. Guo, *ACS Nano*, 2023, **17**, 1610-1621.